Generalized Nambu–Jona-Lasinio model in a study of the boson-exchange model of nuclear forces

C. M. Shakin, Wei-Dong Sun, and J. Szweda

Department of Physics and Center for Nuclear Theory, Brooklyn College of the City University of New York, Brooklyn, New York 11210

In this paper we discuss the role of chiral symmetry in the description of the nucleon-nucleon interaction. We make use of a generalized Nambu–Jona-Lasinio model which exhibits chiral symmetry at the quark level and demonstrate how the various components of the boson-exchange model of the nucleon-nucleon interaction arise in this model. In this paper we make use of our recent analysis of correlated two-pion exchange. We have found that when correlated two-pion exchange is represented by an effective low-mass sigma meson, that meson may be seen to be the chiral partner of the pion. (That result pertains if the meson momentum q is spacelike such that $t=q^2<0$.) We give particular attention to the vertex functions appearing in the boson-exchange model. For monopole forms of the vertex functions the cutoff parameter Λ^{OBE} varies from about 1.3 GeV to 2.0 GeV. In our model the nucleon form factors are characterized by a parameter λ. We show how large cutoff parameters, such as Λ^{OBE}, can arise in our analysis *even if the meson-nucleon vertex is soft, with a characteristic cutoff of about 800 MeV*. We present the values of λ that puts the NJL analysis in good agreement with the boson-exchange model of the nucleon-nucleon force.

I. INTRODUCTION

There has been an ongoing interest in understanding the role of chiral symmetry in nuclear structure studies [1] and in the nucleon-nucleon interaction [2–5]. Some effort has been devoted to introducing chiral symmetry at the level of nucleons and mesons [2–4]; however, the results of that program have been somewhat inconclusive. It is our belief that chiral symmetry is best studied at the quark level by making use of models such as that of Nambu–Jona-Lasinio (NJL) [6]. We present such a study in this work.

We note that the most highly developed and detailed description of the nucleon-nucleon interaction is that of the boson-exchange model [7]. That model makes no reference to chiral symmetry. The essential features of the model are seen in Fig. 1. There we show a linear equation for the nucleon-nucleon T matrix with an interaction, V_{NN}, given by the exchange of mesons ($\sigma,\pi,\rho,\omega,...$). There are form factors at the meson-nucleon vertices that are often taken to have a monopole form. For example,

$$F_\pi(t) = \frac{\Lambda_\pi^2 - m_\pi^2}{\Lambda_\pi^2 - t} \qquad (1.1)$$

may be used at each vertex in the case the pion is exchanged [7]. Here $t=q^2$ is the square of the meson momentum.

Let us concentrate on the most important mesons: σ,π,ρ,ω. For each meson we need to specify the corresponding value of Λ^{OBE}, the coupling constant, and the meson mass. For the ω and ρ mesons, one also needs the ratios (f_ω/g_ω) and (f_ρ/g_ρ) that describe the relative importance of the vector and tensor parts of the meson-nucleon coupling [7]. The π, ρ, and ω mesons are assigned their experimental masses. Therefore, there are at least ten parameters to be specified in the one-boson exchange model.

Since the boson-exchange model provides a detailed description of the nucleon-nucleon force [7] and, since it has

been extensively used to study the properties of nuclear matter [8], it is useful to consider whether such a model is related to a theory with chiral symmetry. The easiest approach to this problem is to attempt to understand the boson-exchange model using a model, such as the NJL model, that has chiral symmetry at the quark level. The NJL model is limited since it does not provide a model of confinement. However, in previous work we have shown how confinement may be introduced [9,10].

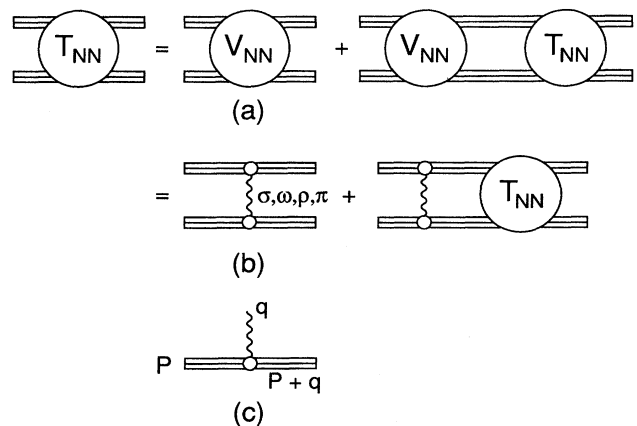One difficulty faced in our program lies in understanding the nature of the sigma meson. Since there is no low-mass

FIG. 1. (a) A linear equation that serves to determine the nucleon-nucleon T matrix is shown. (b) The potential, V_{NN}, is shown for the boson-exchange model, where the important mesons are σ, π, ρ, and ω [7]. The open circles denote phenomenological meson-nucleon vertex functions. (c) The vertex function, $F(q^2)$, is shown for a meson of momentum q. See [7] for a description of the various choices that have been made for the vertex function in boson-exchange models.

sigma in the data tables, the sigma is usually interpreted as an effective meson describing correlated two-pion exchange [11–15]. In a recent work [16] we have made a study of the quark-quark T matrix of the NJL model. We have shown that, for $t = q^2 > 0$, the imaginary part of the T matrix has its origin in correlated two-pion exchange. However, for $t < 0$, the *same* T matrix describes the exchange of the chiral partner of the pion. This feature of our work will be reviewed in the next section.

Since the NJL model, upon bosonization, will describe the various mesons that play an important role in the boson-exchange potentials, we will study that model in some detail. Our procedure involves the following steps. First, we write the one-boson exchange (OBE) amplitude in the various channels. That amplitude is given in terms of the mass of the exchanged meson, the vertex cutoff Λ, and a coupling constant g. (For example, in the case of the pion, the parameters are m_π, Λ_π, and $g_{\pi NN}$.) It is important to note that we do not ascribe any particular physical significance to the individual factors of the OBE amplitude, but consider the amplitude as a whole. As a next step we write the scattering amplitude for the NJL model. Here the various terms are of physical significance. In particular, the NJL amplitude is expressed in terms of the quark-quark T matrix of that model and (physical) form factors of the nucleon. We choose to use a monopole form for the nucleon form factors which are then parametrized by a constant λ. In this work we are mainly concerned with the rate of fall off of the amplitudes with increasing $-q^2$, so that we compare amplitudes that are normalized to 1 for $q^2 = 0$.

As a final step we ask if the NJL amplitudes reproduce the OBE amplitudes in each channel. We find excellent agreement between the phenomenological (OBE) and theoretical (NJL) amplitudes in this case when we take λ to be a free parameter and find the value of λ that puts the NJL and OBE amplitudes in agreement. Such fits are nontrivial since we are attempting to match two functions of q^2 with the choice of a single parameter.

The plan of our work is as follows. In Sec. II, we provide a review of our study of a generalized version of the NJL model and of correlated two-pion exchange [16]. In Sec. III, we consider the quark-quark interaction that is here assumed to mediate the nucleon-nucleon interaction. We provide a $1/n_c$ analysis of the various diagrams that contribute to the interaction and show that, for $t \leq 0$, the most important diagrams correspond to the exchange of $q\bar{q}$ pairs (mesons). For $t > 0$, however, our analysis is consistent with the picture of correlated two-pion exchange (developed at the quark level). In Secs. IV–VI we study meson-exchange processes in the σ, π, ρ, and ω channels. In these sections we attempt to understand why Λ^{OBE} is large (about 1.3–1.7 GeV) while the physical meson-nucleon vertex form factors can be "soft," with a characteristic mass of about 0.8 GeV.

The issue of "soft form factors" has been given a good deal of attention recently [17–19]. For example, in [17], the use of a "soft" form factor in the case of pion exchange requires the introduction of another meson, a π' of mass of about 1.2 GeV. For this massive meson to have any significant role in the t channel that has pion quantum numbers it must be assigned a very large value of $g^2_{\pi' NN}/4\pi$

~ 70–100. This value is much larger than $g^2_{\pi NN}/4\pi \sim 14$ and appears to us to be unrealistic.

A recent work by Flender and Gari [20] reports a nonperturbative and self-consistent determination of baryonic vertex form factors. They find $\lambda_\pi = 0.80$ GeV, $\lambda_\epsilon = 0.50$ GeV, and $\lambda_\omega = 0.60$ GeV. Further, $\lambda_\rho = 0.92$ GeV or 0.61 GeV for the Dirac and Pauli parts of the vertex form factor, respectively. (Note that the ω coupling to the nucleon is almost entirely of vector character, so that only a single value of λ_ω need be given.) The authors of [20] note that the small values of λ they find are quite incompatible with the large values of Λ^{OBE} used in the one-boson-exchange model. In our work we show how this problem may be resolved, so that the "soft" form factors are seen to be consistent with large values of Λ^{OBE}. (Our analysis shows that one should not identify the *physical* parameter λ appearing in the meson-nucleon vertex form factor with the parameter Λ^{OBE}.) In Secs. IV–VI we discuss the relation between λ and Λ^{OBE} in the case of the pion, sigma, rho, and omega mesons. Finally, Sec. VII contains some further discussion and some conclusions.

II. A GENERALIZED NJL MODEL

In a number of works we have studied a coupled-channel quark-hadron model based upon the NJL model [9,21,23]. In that body of work we have included a model of confinement that serves to eliminate unphysical cuts that arise if quarks and antiquarks go on mass shell [10]. Here, we provide a short review of our procedures, since the remainder of our discussion will make use of various elements of our generalized model.

We begin by specifying the form of the quark-quark T matrix in a simple version of the NJL model, where the Lagrangian is

$$\mathcal{L}(x) = \bar{q}(x)(i\gamma^\mu \partial_\mu - m_q^0)q(x) + \frac{G_S}{2}\{[\bar{q}(x)q(x)]^2$$

$$+ [\bar{q}(x)i\gamma_5\vec{\tau}q(x)]^2\} - \frac{G_V}{2}\{[\bar{q}(x)\gamma_\mu\vec{\tau}q(x)]^2$$

$$+ [\bar{q}(x)\gamma_\mu\gamma_5\vec{\tau}q(x)]^2\}, \tag{2.1}$$

if we use the SU(2)-flavor group. Here, m_q^0 is the average current quark mass. The T matrix in the scalar-isoscalar channel is

$$t_{qq}(t) = -\frac{G_S}{1 - G_S J_S(t)}, \tag{2.2}$$

where, with $t = P^2$,

$$J_S(P^2) = (-1)n_c n_f i \int \frac{d^4k}{(2\pi)^3} iS_F(P/2 + k)iS_F(-P/2 + k) \tag{2.3}$$

is the basic quark-loop integral of the NJL model. (See Fig. 2.)

In our generalized NJL model we introduced a model of confinement. That led to a modified form for $J_S(P^2)$. In Fig. 2(a) we show the summation of a ladder of confining interactions [10]. We also define a vertex for the confining field
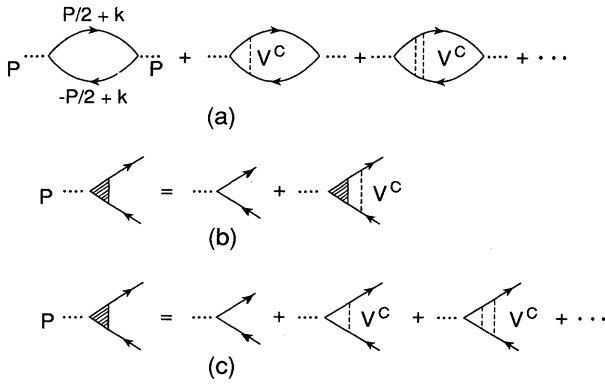
FIG. 2. (a) The diagram on the left is the basic quark loop integral of the NJL model. The propagators are $S_F(p)=(\not p-m_q+i\epsilon)^{-1}$, where m_q is the constituent quark mass. The additional diagrams show the introduction of a confining potential, V^C. (b) A vertex function for the confining interaction (crosshatched area) is given by the equation shown [10]. (c) Here the various terms summed in the equation of (b) are shown.

that satisfies the equation shown in a schematic fashion in Fig. 2(b). [Figure 2(c) exhibits the series that is summed in forming the vertex function.] Once the vertex function is calculated, we can replace $J_S(P^2)$ of Eq. (2.3) by $\hat{J}_S(P^2)$ shown in Fig. 3(b). Note that $\hat{J}_S(P^2)$ does not have an imaginary part that would arise in a theory without confinement when both the quark and antiquark go on mass shell.

Also important for our work is the function $K_S(P^2)$ shown in Fig. 3(c). There, the wavy lines denote pions. Introduction of confinement replaces $K_S(P^2)$ by $\hat{K}_S(P^2)$, shown in Fig. 3(d). Note that $\hat{K}_S(P^2)$ has an imaginary part for $P^2 \geqslant 4m_\pi^2$, since both pions can be on mass shell in that region.

The functions $\hat{J}_S(P^2)$ and $\hat{K}_S(P^2)$ arise when solving coupled equations of the type shown in Fig. 4. Various approximations may be used in solving such equations [9]. Relatively simple results are obtained if the coupling of the $q\bar{q}$ channels to the two-pion continuum is as shown in Fig. 4(b).

We have studied models that we have designated as B and C [9]. In model C, the $q\bar{q}$ T matrix in the scalar-isoscalar channel is

$$t_{qq}^C(t)=-\frac{G_S}{1-G_S\hat{J}_S(t)-G_S\hat{K}_S(t)}.\qquad(2.4)$$

This result has a straightforward diagrammatic representation. For model B, the result is

$$t_{qq}^B(t)=-\frac{G_S[1+G_S\hat{K}_S(t)]}{1-G_S[1+G_S\hat{K}_S(t)]\hat{J}_S(t)}\qquad(2.5)$$

$$=-\frac{G_S'(t)}{1-G_S'(t)\hat{J}_S(t)},\qquad(2.6)$$

with $G_S'(t)=1+G_S\hat{K}_S(t)$. The T matrices, $t_{qq}^B(t)$ and $t_{qq}^C(t)$, are rather similar since $G_S\hat{K}_S(t)$ is small.
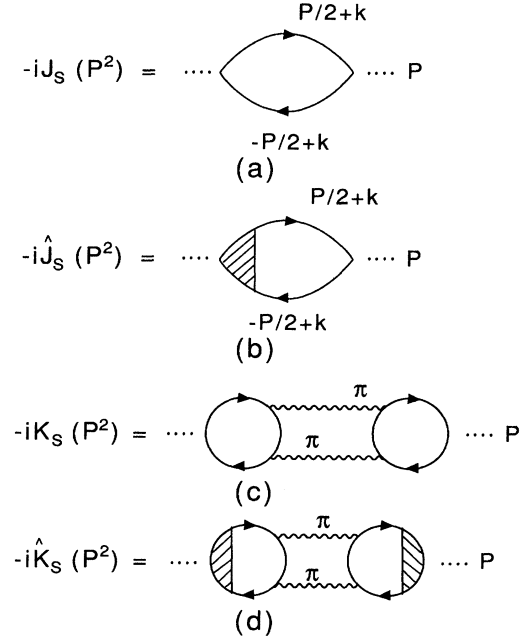

FIG. 3. (a) The basic quark-loop integral of the NJL model is shown. In the notation of this work we have $P^2=t$. [See Eq. (2.3).] (b) The function $\hat{J}_S(P^2)$ is defined by introducing a vertex (crosshatched area) for the confining interaction V^C. See [10] for a detailed discussion of the construction of such vertex functions. (c) The function $K_S(P^2)$ is defined by the diagram shown. (See [9].) (d) The function $\hat{K}_S(P^2)$ is defined by including a vertex function for the confining interaction (cross-hatched region). (See [10].)
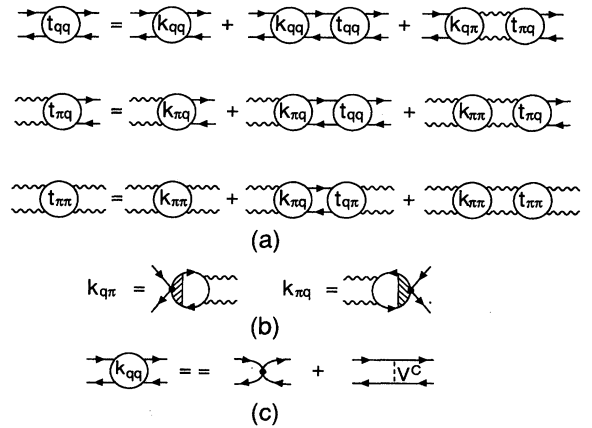

FIG. 4. (a) General form of coupled equations for the T matrices t_{qq}, $t_{q\pi}$, and $t_{\pi\pi}$. (See [20].) (b) The form of the kernels, $k_{q\pi}$ and $k_{\pi q}$, used in our work is shown. (c) The interaction k_{qq} is shown to be composed of the Born term of the NJL model (solid dot) and a confining field V^C.
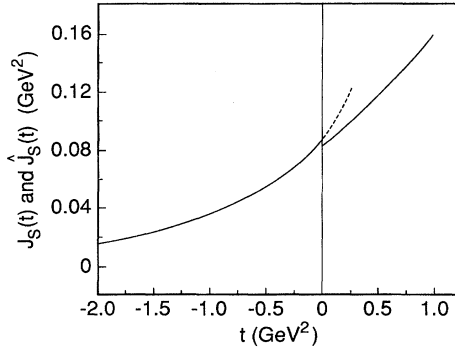
FIG. 5. The dashed line and the solid line for $t<0$ denote the values of $J_S(t)$ calculated in a Euclidean momentum space with $\Lambda_E=1.0$ GeV. The solid line for $t>0$ represents the result of a calculation of $\hat{J}_S(t)$ in Minkowski space. There, a three-dimensional cutoff of $\Lambda_3=0.702$ GeV is used for all the momentum vectors in the integral. Here we use $m_q=262$ MeV, $G_S=7.91$ GeV^{-2} and the model of confinement described in [10]. Note that the inclusion of the confinement vertex function hardly affects the result for $t<0$.

In Fig. 5 we show $\hat{J}_S(t)$ as calculated in an earlier work [16]. The dashed line and the solid line for $t<0$ represent $J_S(t)$, while the solid line for $t>0$ represents $\hat{J}_S(t)$. Note that confinement plays only a minor role for $t<0$ where $\hat{J}_S(t)\simeq J_S(t)$. However, for $t>0$, $\hat{J}_S(t)$ rises more slowly than $J_S(t)$ with increasing t. That has the effect of pushing the scalar-isoscalar resonance to higher energies. For example, in the theory without confinement $m_\sigma\simeq540$ MeV, while with confinement, $m_\sigma>900$ MeV. Therefore, our generalized model is consistent with the fact that there is no low-mass *physical* sigma meson. However, for $t<0$ we have seen that confinement plays only minor role with the consequence that the theory behaves *as if* there was a low-mass sigma, with $m_\sigma\simeq540$ MeV. This result is particularly important for studies of nucleon-nucleon scattering and nuclear structure where the meson momenta are *spacelike*.

In Fig. 6 we exhibit values of Re$\hat{M}_S(P^2)$ and Im$\hat{M}_S(P^2)$, where $\hat{M}_S(P^2)\equiv-G_S^2\hat{K}_S(P^2)$. Since we have calculated values for $\hat{J}_S(t)$ and $\hat{K}_S(t)$, we may present values for $t_{qq}^B(t)$, defined above. In Fig. 7, we show Re$t_{qq}^B(t)$ and Im$t_{qq}^B(t)$. The imaginary part arises from the cuts in the function $\hat{K}_S(t)$. Thus, for $t>0$, $t_{qq}(t)$ describes "correlated two-pion exchange" as defined in [16], for example. The dotted curve in Fig. 7 represents $g^2/(t-m_\sigma^2)$ with $g=3.05$ and $m_\sigma=0.542$ GeV. (Here we have used $G_S=7.91$ GeV^{-2} and $m_q=262$ MeV.) Note that the dotted curve provides a good fit to $t_{qq}^B(t)$ for -0.25 GeV$^2<t<0$, a range of values particularly important for nuclear structure studies. Figure 8 serves to compare the values of $t_{qq}^B(t)$ and $t_{qq}^C(t)$. It may be seen that these functions are very close in value for $t<0$.

III. DIAGRAMMATIC ANALYSIS OF THE NUCLEON-NUCLEON INTERACTION AND $1/n_c$ COUNTING

There are a large number of diagrams that contribute to the calculation of the quark-quark T matrix. We will call the general T matrix T_{qq}, while using t_{qq} to denote the T matri-
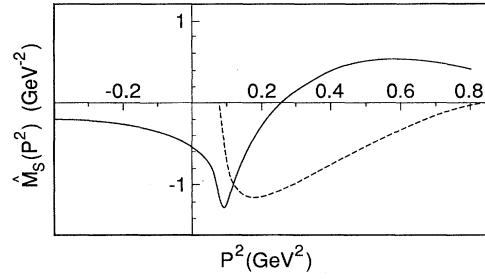

FIG. 6. The function Re$\hat{M}_S(P^2)$ is shown as a solid line. The dashed line is Im$\hat{M}_S(P^2)$. Note that $\hat{M}_S(P^2)=-G_S^2\hat{K}_S(P^2)$. (This figure is taken from [9].)

ces that may be expressed in terms of $\hat{J}_S(t)$ and $\hat{K}_S(t)$ only. [See Eqs. (2.4) and (2.5).] While the various diagrams may be calculated explicitly, it is useful to find some guidance in an organization of the diagrams in powers of $1/n_c$. In that type of counting G_S is of order $1/n_c$ and $\hat{J}_S(t)$ is of order n_c. Further, $g=g_{\sigma qq}=g_{\pi qq}$ is of order $1/\sqrt{n_c}$, while $\hat{K}_S(t)$ is of order unity. Thus, while $G_S\hat{J}_S(t)$ is of order unity, $G_S\hat{K}_S(t)$ is of order $1/n_c$. Indeed, at $t=0$, $G_S\hat{K}_S(0)/G_S\hat{J}_S(0)$ $\simeq-\hat{M}_S(0)/G_S^2\hat{J}_S(0)\simeq0.55/(7.91)^2(0.082)\simeq0.11$, where we have used $\hat{M}_S(t)=-G_S^2\hat{K}_S(t)$ and the values shown in Figs. 5 and 6. (In this case, the result of our calculation is in accordance with what one would expect from $1/n_c$ counting.)

In Fig. 9 we show various diagrams that contribute to the nucleon-nucleon interaction, assumed to be mediated by T_{qq}. In Fig. 9(a) we show some Born terms, where the wavy lines denote pions. The Born diagrams are of order $1/n_c^2$. Of still higher order is the last diagram that involves the pion-pion interaction $t_{\pi\pi}$. (Models for $t_{\pi\pi}$ have been given in Ref. [24]. Some of the terms that contribute to $t_{\pi\pi}$ are shown in
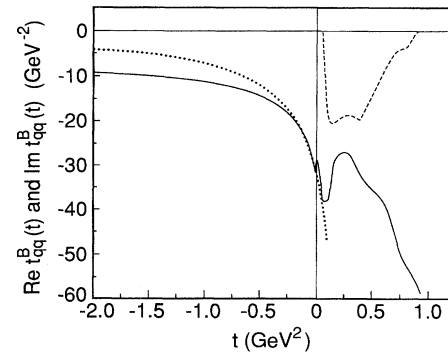

FIG. 7. The figure exhibits Re$t_{qq}(t)$ (solid line) and Im$t_{qq}(t)$ (dashed line) obtained using model B where $t_{qq}(t)$ is given by Eq. (2.5). The dotted line represents $g^2/(t-m_\sigma^2)$ with $g=3.05$ and $m_\sigma=0.542$ GeV. The values for $\hat{J}_S(t)$ to be inserted in Eq. (2.5) are taken from Fig. 5. [We put $\hat{J}_S(t)=J_S(t)$ for $t<0$.] Note that if we were to neglect $\hat{K}_S(t)$, we would have $t_{qq}(0)\simeq-23$ GeV^2. The dotted curve provides a good fit to the solid curve for -0.2 GeV$^2<t\leq0$. This is the range of momentum transfer that is particularly important for nuclear structure physics and for nucleon-nucleon scattering. (This figure is taken from [16].) The small discontinuity in the solid line at $t=0$ is due to the discontinuity in the solid line in Fig. 5.
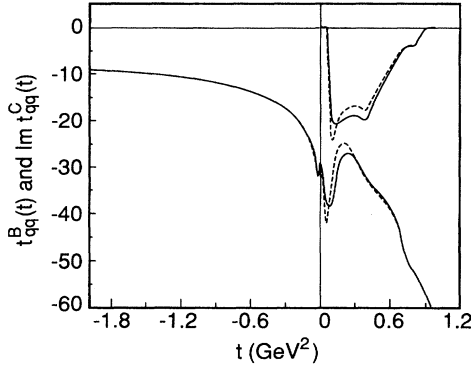
FIG. 8. Values of $t^{B}_{qq}(t)$ (solid line) and $t^{C}_{qq}(t)$ (dashed line) are compared. The curves in the upper right are the imaginary parts and the other curves represent the real parts of $t^{B}_{qq}(t)$ and $t^{C}_{qq}(t)$. It is seen that the real parts are quite similar for $t<0$. The values of Re $t^{B}_{qq}(t)$ and Im $t^{B}_{qq}(t)$ are the same as those shown in Fig. 7.

Fig. 10. The terms depicted in Figs. 10(b)–10(d) have been considered in Ref. [24].)

In Fig. 9(b) we show the contributions that are of order $1/n_c$. The terms shown in Fig. 9(c) are of order $1/n_c^2$, since they contain two factors of G_S, one factor of $\hat{K}_S(t)$ and an arbitrary number of factors of $G_S\hat{J}_S(t)$. Note that the diagrams of Fig. 9(b) are real, while those of Figs. 9(a) and 9(c) have imaginary parts if $t\geq 4m_{\pi}^2$. In Fig. 11(a) we show how we may calculate Im T_{qq} using the diagrams of Fig. 9(c)
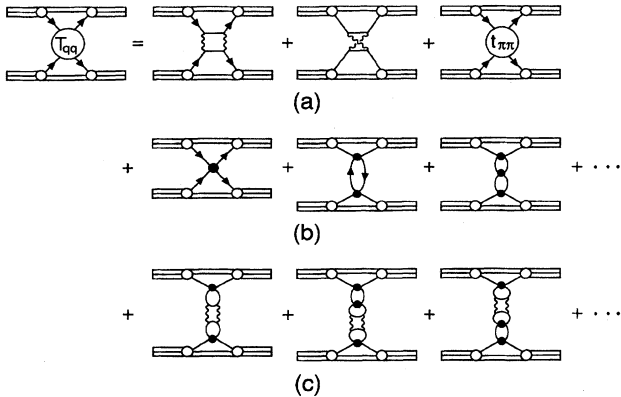

FIG. 9. The figure shows various diagrams that contribute to the quark-quark T matrix, T_{qq}. (a) These diagrams represent Born terms in the quark-quark amplitude and also a term in which the pions interact via a pion-pion interaction $t_{\pi\pi}$. (Models for $t_{\pi\pi}$ may be found in [24].) The first two diagrams in (a) are of order $1/n_c^2$ and the last is of order $1/n_c^3$. (b) Here the solid dot is the basic quark-quark interaction of the NJL model. The remaining diagrams are given in terms of an expansion of the T matrix in powers of $G_S\hat{J}_S(t)$, if we consider the scalar-isoscalar channel, for example. These diagrams are of order $1/n_c$. (c) Diagrams that contain one factor of $\hat{K}_S(t)$, for example, and any number of factors of $G_S\hat{J}_S(t)$. The presence of $\hat{K}_S(t)$ causes these diagrams to be of order $1/n_c^2$. Note that, if we are interested in the imaginary part of $T_{qq}(t)$ for $t>4m_{\pi}^2$, it is the diagrams of (c) that are most important. [Recall that $\hat{J}_S(t)$ is real.]
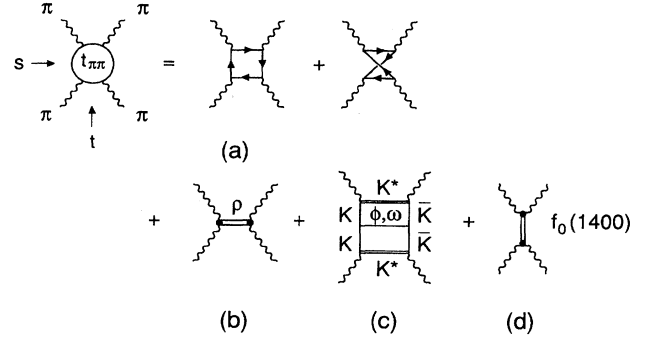

FIG. 10. Various diagrams contributing to a model for $t_{\pi\pi}$ are shown. Here we concentrate on the dynamics in the t channel. (a) Some box and crossed-box diagrams are shown. (b) s-channel ρ exchange is seen to affect the interaction in the t channel for $t_{\pi\pi}$ [24]. (c) Coupling to the $K\bar{K}$ system is important for the description of the resonance $f_0(975)$ in the model of [24]. The $K\bar{K}$ interaction is attractive due to ϕ and ω exchange in that model. (d) The distant resonance, $f_0(1400)$, plays some role in the model of [24].

when $t\geq 4m_{\pi}^2$. In Fig. 11(b) we show a sigma-dominance approximation to the series in Fig. 11(a).

Finally, in Fig. 12 we consider the case $t<0$ and exhibit the leading diagrams which are of order $1/n_c$. At that order, the result is expressed solely in terms of $\hat{J}_S(t)\simeq J_S(t)$,

$$T_{qq}(t)\simeq\frac{-G_S}{1-G_S J_S(t)}.\qquad(3.1)$$

Again, if $-t$ is not too large, we have, for $t<0$,
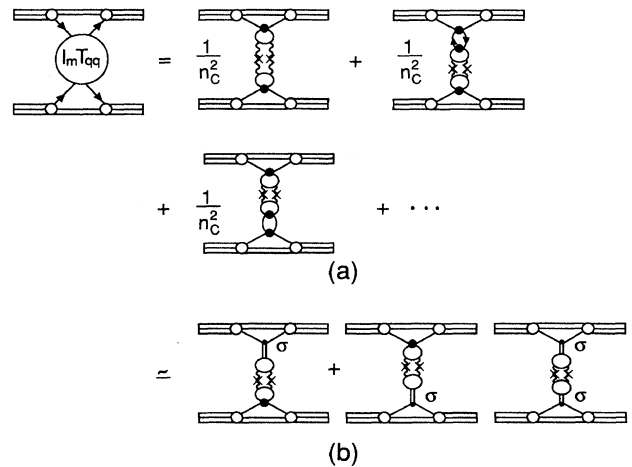

FIG. 11. Diagrams contributing to Im $T_{qq}(t)$ for $t>4m_{\pi}^2$. (a) Diagrams of order $1/n_c^2$ are obtained if a single factor of $\hat{K}_S(t)$ appears. The crosses on the pion lines denote on-mass-shell pions. An arbitrary number of factors of $G_S\hat{J}_S(t)$ may be included. (b) A sigma-dominance approximation to the sum of the amplitudes considered in (a). (See Fig. 7.)
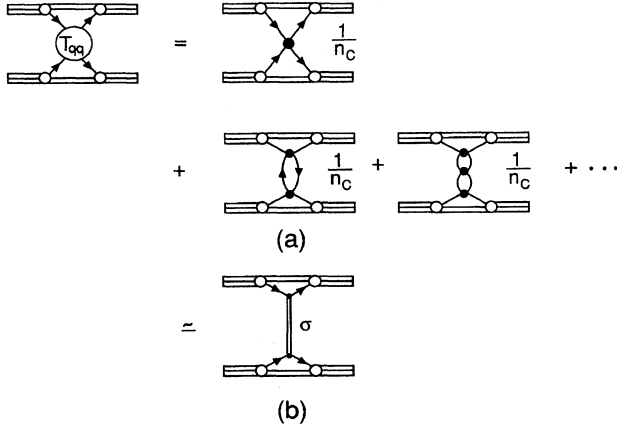
FIG. 12. (a) For $t<0$, the leading terms in the calculation of $T_{qq}(t) \simeq t_{qq}(t)$ are shown. (b) The sum of the diagrams in (a) may be given in terms of a sigma-dominance model if $-t$ is not too large. (See Fig. 7, for example.)

$$T_{qq}(t) = \frac{g^2(t)}{t - m_\sigma^2(t)} \qquad (3.2)$$

$$\simeq \frac{g^2}{t - m_\sigma^2}. \qquad (3.3)$$

[See Fig. 12(b).]

While our discussion here has mainly concerned the scalar-isoscalar t-channel dynamics, we can generalize the discussion to other channels. That will be done in the following sections. However, before leaving this section, it is worth noting that, while the calculation of the diagrams of Fig. 9(a) requires the knowledge of the *quark density matrix of the nucleon*, the calculation of the diagrams of Figs. 9(b) and 9(c) require only the specification of *valence quark form factors* of the nucleon. These form factors are functions of the single variable $t = q^2$.

IV. PION EXCHANGE IN A GENERALIZED NJL MODEL AND IN THE BOSON-EXCHANGE MODEL

Consider the nucleon-nucleon interaction that involves the exchange of $q\bar{q}$ pairs with the quantum numbers of the pion. The T matrix in the NJL model takes the form

$$t_{qq}^{(\pi)}(t) = -\frac{G_S}{1 - G_S \hat{J}_P(t)}, \qquad (4.1)$$

where $\hat{J}_P(t)$ is the appropriate quark-loop integral (see Fig. 13) and where $1 - G_S \hat{J}_P(m_\pi^2) = 0$. Using a momentum-space bosonization procedure [25], we have

$$-\frac{G_S}{1 - G_S \hat{J}_P(t)} = \frac{g_{\pi qq}^2(t)}{t - m_\pi^2(t)} \qquad (4.2)$$

at one-loop order.
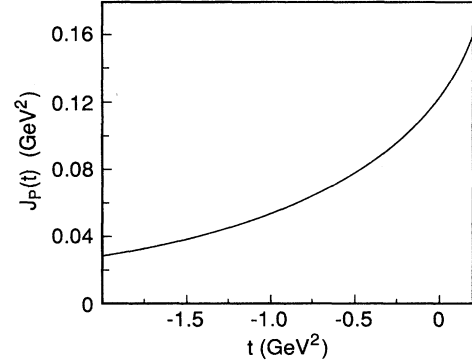
If $|t|$ is not too large, we may use the approximation

FIG. 13. The function $J_P(t)$ is shown. The calculation is made by using a Euclidean momentum space. Here $m_q = 0.262$ GeV and $G_S = 7.91$ GeV^{-2}.

$$\frac{g_{\pi qq}^2(t)}{t - m_\pi^2(t)} \simeq \frac{g_{\pi qq}^2(0)}{t - m_\pi^2(0)} \qquad (4.3)$$

$$= \frac{g_{\pi qq}^2}{t - m_\pi^2}, \qquad (4.4)$$

where $g_{\pi qq} \equiv g_{\pi qq}(0)$ and $m_\pi \equiv m_\pi(0)$. (See Fig. 7, for example.)

Now, the leading diagrams that are of order $1/n_c$ yield the interaction

$$V_\pi(t) = t_{qq}^{(\pi)}(t) \tilde{F}_\pi^2(0) \left(\frac{\lambda_\pi^2}{\lambda_\pi^2 - t} \right)^2. \qquad (4.5)$$

Here $t_{qq}^{(\pi)}(t)$ is given by Eq. (4.1) or Eq. (4.2) and $\tilde{F}_\pi(0)[\lambda_\pi^2/(\lambda_\pi^2 - t)]$ is the valence form factor of the nucleon in the pion channel corresponding to the diagrams of Fig. 12. The parameter $\tilde{F}_\pi(0)$ is defined via the relation

$$\tilde{F}_\pi(0) \left(\frac{\lambda_\pi^2}{\lambda_\pi^2 - t} \right) \bar{u}(\vec{P} + \vec{q}, s') \gamma_5 u(\vec{P}, s) \langle \tau' | \vec{\tau} | \tau \rangle$$

$$= \langle N, \vec{P} + \vec{q}, s', \tau' | \bar{q}(0) \gamma_5 \vec{\tau} q(0) | N, \vec{P}, s, \tau \rangle_{\text{val}}. \qquad (4.6)$$

Now let us identify $V_\pi(t)$ of Eq. (4.5) with $V_\pi^{\text{OBE}}(t)$, where

$$V_\pi^{\text{OBE}}(t) = \frac{g_{\pi NN}^2}{t - m_\pi^2} \left(\frac{\Lambda_\pi^2 - m_\pi^2}{\Lambda_\pi^2 - t} \right)^2, \qquad (4.7)$$

with $g_{\pi NN}^2/4\pi \simeq 14.4-14.9$ and $\Lambda_\pi^{\text{OBE}} \sim 1.3$ GeV to 1.4 GeV [7]. Thus, we should have

$$\frac{g_{\pi NN}^2}{t - m_\pi^2} \left(\frac{\Lambda_\pi^2 - m_\pi^2}{\Lambda_\pi^2 - t} \right)^2 = t_{qq}^{(\pi)}(t) \tilde{F}_\pi^2(0) \left(\frac{\lambda_\pi^2}{\lambda_\pi^2 - t} \right)^2 \qquad (4.8)$$

for $t<0$. For example, if we use Table A.1 of [7], we have $g_{\pi NN}^2/4\pi = 14.7$ and $\Lambda_\pi = 1.3$ GeV. If we further put $g_{\pi qq} = 2.72$ and $m_\pi = 138$ MeV, we see that we should have
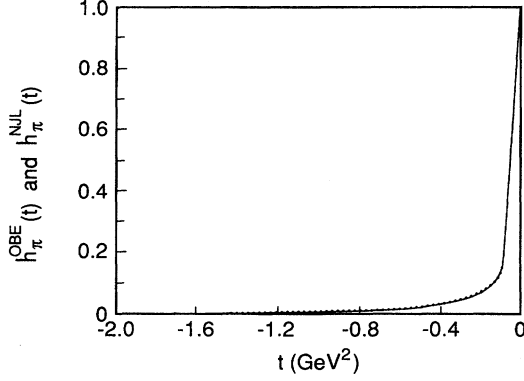
FIG. 14. Values of $h_\pi^{\mathrm{NJL}}(t)$ are given by the solid line and $h_\pi^{\mathrm{OBE}}(t)$ is represented by the dotted line. Here $\lambda_\pi = 0.80$ GeV and $\Lambda_\pi^{\mathrm{OBE}} = 1.3$ GeV [7]. (See Fig. 15.)

$\tilde{F}_\pi(0) = 4.97$ if Eq. (4.8) is to be valid. Since we have not calculated $\tilde{F}_\pi(0)$ at this point, we will compare the rates of fall with increasing $-t$ of the two sides of Eq. (4.8). To that end, we define

$$h_\pi^{\mathrm{OBE}}(t) = \left(\frac{m_\pi^2}{g_{\pi NN}^2}\right)\left(\frac{\Lambda_\pi^2}{\Lambda_\pi^2 - m_\pi^2}\right)^2 \frac{(-g_{\pi NN}^2)}{t - m_\pi^2}\left(\frac{\Lambda_\pi^2 - m_\pi^2}{\Lambda_\pi^2 - t}\right)^2 \tag{4.9}$$

and

$$h_\pi^{\mathrm{NJL}}(t) = \frac{t_{qq}^{(\pi)}(t)}{t_{qq}^{(\pi)}(0)}\left(\frac{\lambda_\pi^2}{\lambda_\pi^2 - t}\right)^2, \tag{4.10}$$

which are defined such that $h_\pi^{\mathrm{OBE}}(0) = h_\pi^{\mathrm{NJL}}(0) = 1$.

In Figs. 14 and 15 we show $h_\pi^{\mathrm{NJL}}(t)$ of Eq. (4.10) as a solid line. (Here $\lambda_\pi = 0.8$ GeV.) Also shown, as a dotted line, is $h_\pi^{\mathrm{OBE}}(t)$ with $\Lambda_\pi = 1.3$ GeV, $m_\pi = 0.138$ GeV, and $g_{\pi NN}^2/4\pi = 14.7$. For small negative t $(-0.1 < t < 0.0$ GeV$^2)$, the curves are undistinguishable and they are not shown in that region in Fig. 15. (Note that both curves go to 1 at $t = 0$.)

We see that, even though $\lambda_\pi = 0.8$ GeV, we still need $\Lambda_\pi^{\mathrm{OBE}} \approx 1.3$ GeV, if the simple form of the OBE model is used, as in Eq. (4.7). Thus, we infer that while λ_π is a physical parameter, $\Lambda_\pi^{\mathrm{OBE}}$ is not. This result resolves some of the problems described in [20] where values of λ and Λ^{OBE} are compared for a number of mesons.

V. SIGMA EXCHANGE IN THE NJL MODEL AND IN THE BOSON-EXCHANGE MODEL

We have seen how sigma exchange may be used to parametrize the quark T matrix, if $t < 0$ [16]. Proceeding as in Sec. IV, we write

$$t_{qq}^{(\sigma)}(t) = -\frac{G_S}{1 - G_S \hat{J}_S(t)}. \tag{5.1}$$
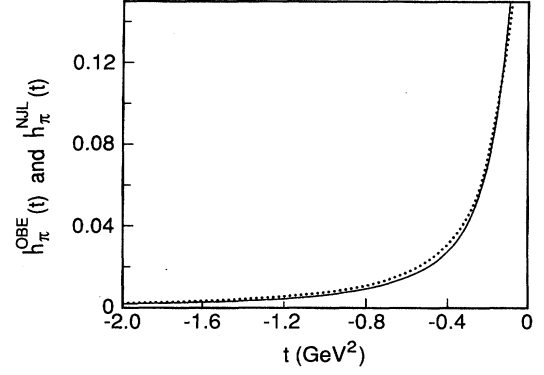
More precisely, we could put

FIG. 15. Values of $h_\pi^{\mathrm{NJL}}(t)$ (solid line) and $h_\pi^{\mathrm{OBE}}(t)$ (dotted line) are shown on an expanded scale relative to Fig. 14. Here $\lambda_\pi = 0.80$ GeV and $\Lambda_\pi^{\mathrm{OBE}} = 1.3$ GeV. Note that, by definition, both curves go to 1 at $t = 0$.

$$t_{qq}^{(\sigma)}(t) = -\frac{G_S}{1 - G_S \hat{J}_S(t) - G_S \hat{K}_S(t)}, \tag{5.2}$$

but we will drop $\hat{K}_S(t)$ as it represents only a small correction to Eq. (5.1) when $t < 0$. Momentum-space bosonization [25] yields the relation

$$-\frac{G_S}{1 - G_S \hat{J}_S(t)} = \frac{g_{\sigma qq}^2(t)}{t - m_\sigma^2(t)} \tag{5.3}$$

for $t < 0$.

Let us define the interaction for the generalized NJL model

$$V_\sigma(t) = t_{qq}^{(\sigma)}(t)\tilde{F}_\sigma^2(0)\left(\frac{\lambda_\sigma^2}{\lambda_\sigma^2 - t}\right)^2, \tag{5.4}$$

where $\tilde{F}_\sigma(0)$ is defined via the relation

$$\tilde{F}_\sigma(0)\left(\frac{\lambda_\sigma^2}{\lambda_\sigma^2 - t}\right)\bar{u}(\vec{P} + \vec{q}, s')u(\vec{P}, s)\delta_{\tau\tau'}$$

$$= \langle N, \vec{P} + \vec{q}, s', \tau' | \bar{q}(0)q(0) | N, \vec{P}, s, \tau\rangle_{\mathrm{val}}. \tag{5.5}$$

For the boson-exchange model we have the interaction

$$V_\sigma^{\mathrm{OBE}}(t) = \frac{g_{\sigma NN}^2}{t - m_\sigma^2}\left(\frac{\Lambda_\sigma^2 - m_\sigma^2}{\Lambda_\sigma^2 - t}\right)^2. \tag{5.6}$$

Thus, as in Eqs. (4.9) and (4.10), we define

$$h_\sigma^{\mathrm{OBE}}(t) = \left(\frac{m_\sigma^2}{g_{\sigma NN}^2}\right)\left(\frac{\Lambda_\sigma^2}{\Lambda_\sigma^2 - m_\sigma^2}\right)^2\left(\frac{-g_{\sigma NN}^2}{t - m_\sigma^2}\right)\left(\frac{\Lambda_\sigma^2 - m_\sigma^2}{\Lambda_\sigma^2 - t}\right)^2 \tag{5.7}$$
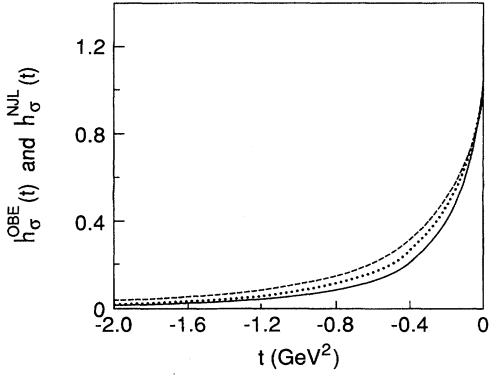
and

FIG. 16. Values for $h_\sigma^{NJL}(t)$ are shown as a solid line for $\lambda_\sigma = 0.80$ GeV and $m_\sigma = 0.54$ GeV. Values of $h_\sigma^{OBE}(t)$ are given for $\Lambda_\sigma = 1.2$ GeV (dotted line) and $\Lambda_\sigma^{OBE} = 1.5$ GeV (dashed line). The value for Λ_σ^{OBE} from [7] is 1.5 GeV, with $m_\sigma = 0.55$ GeV. (This figure would appear essentially the same if model C were used.) Note that if λ_σ is increased to 1.0 GeV the agreement of the solid line with the dashed line ($\lambda_\sigma^{OBE} = 1.5$ GeV) is very good. Almost perfect overlap is obtained if λ_σ is increased to 1.1 GeV.

$$h_\sigma^{NJL}(t) = \frac{t_{qq}^{(\sigma)}(t)}{t_{qq}^{(\sigma)}(0)} \left(\frac{\lambda_\sigma^2}{\lambda_\sigma^2 - t} \right)^2 . \tag{5.8}$$

First let us compare $V_\sigma(t)$ and $V_\sigma^{OBE}(t)$ at $t=0$. We use model I of Table B.1 of [7]. For that model, we have $g_{\sigma NN}^2/4\pi = 6.32$, $m_\sigma = 0.55$ GeV, and $\Lambda_\sigma = 1.5$ GeV. (We use this particular OBE potential since the effects of the excitation of the delta are explicitly separated.) We now equate the interactions at $t=0$:

$$-\frac{g_{\sigma NN}^2}{m_\sigma^2} \left(\frac{\Lambda_\sigma^2 - m_\sigma^2}{\Lambda_\sigma^2} \right)^2 = -\frac{g_{\sigma qq}^2}{m_\sigma^2} [\tilde{F}_\sigma(0)]^2 . \tag{5.9}$$

For $\Lambda_\sigma = 1.5$ GeV, $g_{\sigma NN}^2/4\pi = 6.32$ and $g_{\sigma qq} = 3.05$, we obtain $\tilde{F}_\sigma(0) = 2.54$ from Eq. (5.9). [If we include the effects of a finite value of $G_S \hat{K}_S(0)$, we obtain $\tilde{F}_\sigma(0) = 2.78$ instead of 2.54.] For the nonrelativistic quark model we would have $\tilde{F}_\sigma(0) = 3$, since in that case the same value is obtained for the matrix elements of $q^\dagger(0)q(0)$ and $\bar{q}(0)q(0)$. However, the use of relativistic wave functions (with small components) would lead to $\tilde{F}_\sigma(0) \leq 3$. We expect about a 10% reduction from the value 3, that is $\tilde{F}_\sigma(0) \simeq 2.7$. Therefore, we infer that the NJL model may give a good account of the magnitude of that part of the scalar-isoscalar ($T=0$) potential that does not involve excitation of the delta [7].

We return to a comparison of $h_\sigma^{OBE}(t)$ and $h_\sigma^{NJL}(t)$ of Eqs. (5.7) and (5.8). In Fig. 16 the solid line represents $h_\sigma^{NJL}(t)$. The dotted line represents $h_\sigma^{OBE}(t)$ with $\Lambda_\sigma = 1.2$ GeV and the dashed line represents $h_\sigma^{OBE}(t)$ with $\Lambda_\sigma = 1.5$ GeV. (The value used in [7] is $\Lambda_\sigma = 1.5$ GeV.) If we increase λ_σ to 1.1 GeV, we find essentially perfect agreement with $h_\sigma^{OBE}(t)$ calculated for $\Lambda_\sigma = 1.5$ GeV.

VI. RHO AND OMEGA EXCHANGE IN THE GENERALIZED NJL MODEL AND IN THE OBE MODEL

The discussion of the exchange of the rho and omega mesons is made somewhat more complicated than the dis-

cussion of pion and sigma exchange due to the necessity of specifying two form factors. For example, we have for the isoscalar and isovector parts of the electromagnetic current,

$$\langle N, \vec{P} + \vec{q}, s' \tau' | \bar{q}(0) \frac{\gamma^\mu}{6} q(0) | N, \vec{P}, s \tau \rangle$$

$$= \delta_{\tau\tau'} \bar{u}(\vec{P} + q, s') \left[\gamma^\mu F_{10}(q^2) + \frac{i\sigma^{\mu\nu}}{2m_N} q_\nu F_{20}(q^2) \right] u(\vec{P}, s) \tag{6.1}$$

and

$$\langle N, \vec{P} + \vec{q}, s' \tau' | \bar{q}(0) \frac{\gamma^\mu}{6} q(0) | N, \vec{P}, s \tau \rangle$$

$$= \langle \tau' | \vec{\tau} | \tau \rangle \bar{u}(\vec{P} + \vec{q}, s') \left[\gamma^\mu F_{11}(q^2) + \frac{i\sigma^{\mu\nu}}{2m_N} q_\nu F_{21}(q^2) \right] u(\vec{P}, s) . \tag{6.2}$$

These forms may be used to specify the form factors of the nucleon that are needed to calculate the diagrams of order $1/n_c$. Equation (6.1) is needed for the (isoscalar) ω meson and Eq. (6.2) is needed for the (isovector) ρ meson. [Note that $F_{10}(0) = F_{11}(0) = 1/2$, so that, for the proton form factor, we have $F_1^p(0) = 1$ and for the neutron form factor we have $F_1^n(0) = 0$.]

For omega exchange in the boson-exchange model, we have at each vertex

$$ig_\omega \bar{u}(\vec{P} + \vec{q}, s') \left[\gamma^\mu + \frac{f_\omega}{g_\omega} i \frac{\sigma^{\mu\nu}}{2m_N} q_\nu \right] u(\vec{P}, s) \left(\frac{\Lambda_\omega^2 - m_\omega^2}{\Lambda_\omega^2 - q^2} \right) \delta_{\tau\tau'} , \tag{6.3}$$

if we use monopole vertex cutoffs. In the case of the ω, $f_\omega/g_\omega = 0$ in phenomenological fits.

For rho exchange in the boson-exchange model, we have at each vertex

$$ig_\rho \bar{u}(\vec{P} + \vec{q}, s') \left[\gamma^\mu + \frac{f_\rho}{g_\rho} i \frac{\sigma^{\mu\nu}}{2m_N} q_\nu \right] u(\vec{P}, s) \left(\frac{\Lambda_\rho^2 - m_\rho^2}{\Lambda_\rho^2 - q^2} \right)$$

$$\times \langle \tau' | \vec{\tau} | \tau \rangle . \tag{6.4}$$

In the case of the rho, we have $f_\rho/g_\rho = 6.1$ in standard phenomenological fits, while Λ_ρ is about 1.3 GeV [7]. To keep our analysis simple, we will be interested in the behavior of the vertex functions with increasing $-t = -q^2$. Again let us define the basic quark-loop integral to be $\hat{J}_\rho(t)$ and write

$$t_{qq}^{(\rho)}(t) = \frac{G_V}{1 - G_V \hat{J}_\rho(t)} . \tag{6.5}$$

Values of $\hat{J}_\rho(t)$ are given in [21]. We also define

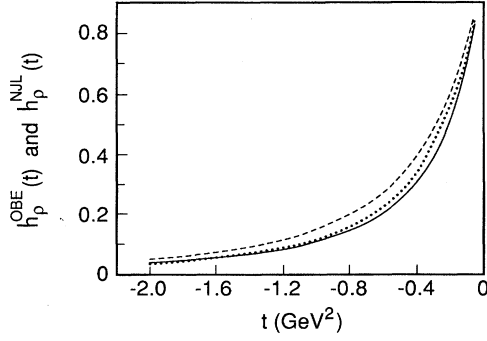$$h_\rho^{NJL}(t) = \frac{t_{qq}^{(\rho)}(t)}{t_{qq}^{(\rho)}(0)} \left(\frac{\lambda_\rho^2}{\lambda_\rho^2 - t} \right)^2 \tag{6.6}$$

FIG. 17. Values of $h_\rho^{NJL}(t)$ are shown as a solid line for $\lambda_\rho = 0.80$ GeV. The dotted line represents $h_\rho^{OBE}(t)$ for $\Lambda_\rho^{OBE} = 1.1$ GeV and the dashed line represents $h_\rho^{OBE}(t)$ when $\Lambda_\rho^{OBE} = 1.3$ GeV. For the calculation of h_ρ^{NJL} we used results of a previous work where we had $G_V = 9.2$ GeV^{-2}, $m_q = 350$ MeV. The Euclidean-space calculation of $J_\rho(t)$ made here had a momentum cutoff $\Lambda_E = 0.68$ GeV.

in analogy to Eq. (4.10), for example, and

$$h_\rho^{OBE}(t) = \left(\frac{m_\rho^2}{g_{\rho NN}^2} \right) \left(\frac{\Lambda_\rho^2}{\Lambda_\rho^2 - m_\rho^2} \right)^2 \left(\frac{-g_{\rho NN}^2}{t - m_\rho^2} \right) \left(\frac{\Lambda_\rho^2 - m_\rho^2}{\Lambda_\rho^2 - t} \right)^2$$

(6.7)

in analogy to Eq. (4.9). Note that $h_\rho^{NJL}(0) = h_\rho^{OBE}(0) = 1$. To compare $h_\rho^{NJL}(t)$ and $h_\rho^{OBE}(t)$ we make use of some calculations of $J_\rho(t)$ made in our study of the vector-isovector current correlation function [21]. In that work we have $m_q = 350$ MeV and $G_V = 9.2$ GeV^{-2}. In the present work we calculate $J_\rho(t)$ for negative t using a Euclidean momentum space with a cutoff $\Lambda_E = 0.680$ GeV. We then use Eq. (6.4) with the approximation that $\hat{J}_\rho(t) \simeq J_\rho(t)$ for $t < 0$. The results of our calculations are shown in Fig. 17. There the solid line represents $h_\rho^{NJL}(t)$. The dotted line represents $h_\rho^{OBE}(t)$ with $\Lambda_\rho = 1.1$ GeV and the dashed line represents $h_\rho^{OBE}(t)$ with $\Lambda_\rho = 1.3$ GeV. Here, we put $\lambda_\rho = 0.8$ GeV in Eq. (6.6). It is seen that the phenomenological value of the cutoff parameter, $\Lambda_\rho = 1.3$ GeV [7], is generally consistent with a "soft" form factor that has $\lambda_\rho = 0.8$ GeV. However, if we increase λ_ρ to 0.93 GeV, we get a significantly better fit. (See Fig. 18 and Table I.)

We remark that for the $1/n_c$ diagrams considered here the theory gives rise to the vector-dominance result $f_\rho/g_\rho = 3.70$, since these diagrams yield an interaction of the form

$$V = -\bar{u}(\vec{P} + \vec{q}, s_2') \left[\gamma^\mu F_{11}(t) + \frac{i\sigma^{\mu\nu} q_\nu}{2m_N} F_{21}(t) \right] u(\vec{P}, s_2)$$

$$\times \left(\frac{G_V}{1 - G_V J_\rho(t)} \right) g_{\mu\alpha} \bar{u}(\vec{P}' - \vec{q}, s_1') \left[\gamma^\alpha F_{11}(t) \right.$$

$$\left. - \frac{i\sigma^{\alpha\beta} q_\beta}{2m_N} F_{21}(t) \right] u(\vec{P}', s_1) \langle \tau_2' | \vec{\tau} | \tau_2 \rangle \cdot \langle \tau_1' | \vec{\tau} | \tau_1 \rangle \quad (6.8)$$

for the NJL diagrams of order $1/n_c$.

In order to check upon the magnitude of $g_{\rho NN}^2/4\pi$ given by our model, we can write

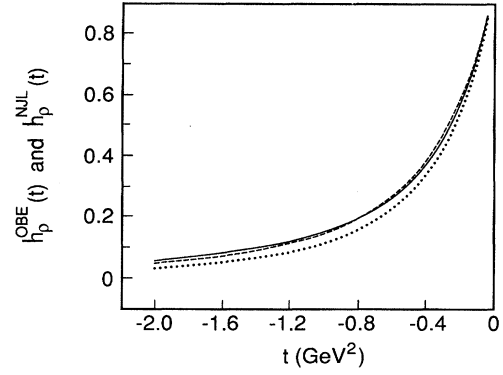FIG. 18. Values of $h_\rho^{NJL}(t)$ are shown as a solid line for $\lambda_\rho = 0.93$ GeV. The dotted line represents $h_\rho^{OBE}(t)$ for $\Lambda_\rho^{OBE} = 1.1$ GeV and the dashed line represents $h_\rho^{OBE}(t)$ for $\Lambda_\rho^{OBE} = 1.3$ GeV. (See caption to Fig. 17 and Table I.)

$$\frac{g_{\rho NN}^2}{4\pi} \left(\frac{\Lambda_\rho^2 - m_\rho^2}{\Lambda_\rho^2} \right)^2 = \frac{g_{\rho qq}^2}{4\pi} .$$

(6.9)

To obtain $g_{\rho qq}^2$, we write the relation that pertains upon bosonization

$$\frac{G_V}{1 - G_V J_\rho(0)} = \frac{g_{\rho qq}^2}{m_\rho^2} .$$

(6.10)

With $G_V = 9.2$ GeV^{-2}, $J_\rho(0) = 0.049$ GeV^2 [22] and $m_\rho = 0.770$ GeV, we find $g_{\rho qq}^2/4\pi = 0.79$ from which we obtain $g_{\rho NN}^2/4\pi = 1.86$ when $\Lambda_\rho = 1.3$ GeV. Values for $g_{\rho NN}^2/4\pi$ range from about 0.95 to 1.2 in the various OBE models that use monopole vertex cutoffs [7]. (Note that a larger value for $g_{\rho qq}$ was quoted in [21] since a different bosonization relation was used there.) We remark that it would be of some interest to see if consideration of additional diagrams would yield values for f_ρ/g_ρ larger than the value of 3.70 obtained here.

We note that $g_{\omega NN} = 3g_{\rho NN}$. Then, it is seen that, if $\Lambda_\rho = \Lambda_\omega$, $g_{\omega NN}^2/4\pi = 9g_{\rho NN}^2/4\pi$ in our model. With the value given above for $g_{\rho NN}^2/4\pi$, we find $g_{\omega NN}^2/4\pi = 16.7$. From Table A.1 of [7], we have $g_{\omega NN}^2/4\pi = 25$ for $\Lambda^{OBE} = 1.35$ GeV. We see, therefore, that the diagrams of order $1/n_c$ provide only about 67% of the repulsion in the ω channel. Study of diagrams of order $1/n_c^2$ may, therefore, be useful in obtaining an improved fit to the phenomenological value of the OBE potential in the ω channel. For a more

TABLE I. Typical values of Λ^{OBE} are given for various mesons [7] as are the values of λ considered here. The items with asterisks denote those values of λ that yield a very accurate fit to $h^{OBE}(t)$ for $t < 0$.

Meson	Λ^{OBE} (GeV)	λ (GeV)	Figure
π	1.3	*0.80	14
σ	1.5	0.80	16
		*1.10	Not shown
ρ, ω	1.3	0.80	17
		*0.93	18

successful calculation of the strength of the interaction for rho and omega exchange, see [26].

VII. DISCUSSION AND CONCLUSION

The large values of Λ^{OBE} of the boson-exchange model have always been somewhat puzzling. In this work we have shown how these values may be understood. It has been seen, within the context of our model, that Λ^{OBE} has no direct physical significance, but is needed to make phenomenological form such as

$$\left(\frac{\Lambda^2 - m^2}{\Lambda^2 - t}\right)^2 \frac{g^2}{t - m^2}$$

follow the behavior of the product of the quark-quark T matrix and the square of the meson-nucleon vertex function for spacelike t. Indeed, in the case of the pion the coincidence of the two functions is remarkable. (See Figs. 14 and 15 and Table I.)

Probably of more significance is the fact that the NJL model exhibits chiral symmetry and provides a basis for deriving the boson-exchange model. The role of chiral symmetry in understanding the origin or the nucleon-nucleon force has been of interest for some time [2–4]. One approach to that problem has been to consider Skyrmion-Skyrmion scat-

tering. However, it is not expected that a detailed description of the force will emerge in such studies. It is also unlikely that one can obtain an understanding of nuclear matter based upon the Skyrmion-Skyrmion interaction. On the other hand, studies of finite nuclei and of nuclear matter based upon the boson-exchange model have been quite successful [8].

It may also be seen from our analysis that a large part of the (Lorentz) scalar field found in nuclei is a chiral field [1]. The magnitude of that field is related to the partial restoration of chiral symmetry at finite density. Thus, it is possible to relate QCD sum-rule studies in matter [1], Dirac phenomenology, and the boson-exchange model in a single formalism that has its base in models that exhibit chiral symmetry at the quark level.

In future work one may study terms of order $1/n_c^2$ to see if the magnitudes of the force in the rho and omega channels can be given more accurately. It will also be of value to calculate λ_σ, λ_ρ, and λ_ω, either in a lattice simulation of QCD, or in a quark model of nucleon structure.

ACKNOWLEDGMENTS

[1] L. S. Celenza, A. Pantziris, C. M. Shakin, and Wei-Dong Sun, Phys. Rev. C **45**, 2015 (1992); L. S. Celenza, A. Pantziris, C. M. Shakin, and Wei-Dong Sun, *ibid.* **46**, 57 (1992); L. S. Celenza, C. M. Shakin, Wei-Dong Sun, and Xiquan Zhu, *ibid.* **48**, 159 (1993). For work dealing with QCD sum rules in matter, see T. D. Cohen, R. J. Furnstahl, and D. K. Griegel, Phys. Rev. Lett. **67**, 961 (1991); T. Hatsuda, H. Høgaasen, and M. Prakash, Phys. Rev. C **42**, 2212 (1990); R. J. Furnstahl, D. K. Griegel, and T. Cohen, *ibid.* **46**, 1507 (1992); X. Jin, T. D. Cohen, R. J. Furnstahl, and D. K. Griegel, *ibid.* **47**, 2882 (1993); X. Jin, M. Nielsen, T. D. Cohen, R. J. Furnstahl, and D. K. Griegel, *ibid.* **49**, 464 (1994); X. Jin and R. J. Furnstahl, *ibid.* **49**, 1190 (1994); X. Jin and M. Nielsen, *ibid.* **51**, 347 (1995); C. M. Shakin, *ibid.* **50**, 1129 (1994).

[2] L. S. Celenza, A. Pantziris, and C. M. Shakin, Phys. Rev. C **46**, 2213 (1992). In this work we calculated the two-nucleon-irreducible matrix elements of the interaction for insertion in a Bethe-Salpeter equation, for example. Therefore, we did not attempt to demonstrate the equivalence of pseudoscalar and pseudovector coupling schemes.

[3] C. A. da Rocha and M. R. Robilotta, Phys. Rev. C **49**, 1818 (1994).

[4] C. Ordonez, L. Ray, and U. van Kolck, Phys. Rev. Lett. **72**, 1982 (1994).

[5] M. Birse, Phys. Rev. C **49**, 2212 (1994).

[6] Y. Nambu and G. Jona-Lasinio, Phys. Rev. **122**, 345 (1961); **124**, 246 (1961).

[7] R. Machleidt, in *Advances in Nuclear Physics*, Vol. 19, edited by J. W. Negele and E. Vogt (Plenum, New York, 1989).

[8] See, for example, L. S. Celenza and C. M. Shakin, *Relativistic Nuclear Physics: Theories of Structure and Scattering* (World Scientific, Singapore, 1986); J. B. Ter Haar and R. Malfliet, Phys. Rep. **149**, 209 (1987). For recent work and additional references see H. Huber, F. Weber, and M. K. Weigel, Phys. Rev. C **51**, 1790 (1995).

[9] L. S. Celenza, C. M. Shakin, Wei-Dong Sun, J. Szweda, and Xiquan Zhu, Int. J. Mod. Phys. E **2**, 603 (1993). In this reference $\text{Re}C(P^2)$ obtained from a dispersion relation should be replaced by $\text{Re}C(P^2) + \hat{J}_S(P^2)$.

[10] L. S. Celenza, C. M. Shakin, Wei-Dong Sun, J. Szweda, and Xiquan Zhu, Phys. Rev. D **51**, 3638 (1995).

[11] G. E. Brown and A. D. Jackson, *The Nucleon-Nucleon Interaction* (North-Holland, Amsterdam, 1976).

[12] J. W. Durso, M. Saavela, G. E. Brown, and B. J. Verwest, Nucl. Phys. **A278**, 445 (1977); J. W. Durso, A. D. Jackson, and B. J. Verwest, *ibid.* **A345**, 471 (1980).

[13] W. Lin and D. B. Serot, Nucl. Phys. **A512**, 637 (1990).

[14] C. Schütz, J. W. Durso, K. Holinde, and J. Speth, Phys. Rev. C **49**, 2671 (1994).

[15] H.-C. Kim, J. W. Durso, and K. Holinde, Phys. Rev. C **49**, 2355 (1994).

[16] L. S. Celenza, C. M. Shakin, Wei-Dong Sun, and J. Szweda, Brooklyn College Report BCCNT 95/032/245, 1995, submitted to Phys. Rev. C.

[17] K. Holinde and A. W. Thomas, Phys. Rev. C **42**, R1195 (1990).

[18] J. Haidenbauer, K. Holinde, and A. W. Thomas, Phys. Rev. C **49**, 2331 (1994).

[19] K. Holinde, Institut für Kernphysik, Forschungszentrum, Jülich, Report No. KFA-IKP(TH)-1994-41, 1994; unpublished.

[20] J. Flender and M. F. Gari, Phys. Rev. C **51**, R1619 (1995).

In this work the mass of the ϵ meson is taken as 975 MeV.

[21] L. S. Celenza, C. M. Shakin, Wei-Dong Sun, J. Szweda, and Xiquan Zhu, Ann. Phys. (N.Y.) **241**, 1 (1995).

[22] C. M. Shakin, Wei-Dong Sun, and J. Szweda, Ann. Phys. (N.Y.) **241**, 37 (1995).

[23] L. S. Celenza, C. M. Shakin, and J. Szweda, Int. J. Mod. Phys. E **2**, 437 (1993).

[24] D. Lohse, J. W. Durso, K. Holinde, and J. Speth, Nucl. Phys. **A516**, 513 (1990).

[25] We find the momentum-space bosonization scheme of V. Bernard, A. A. Osipov, and Ulf-G. Meissner, Phys. Lett. B **285**, 119 (1992), to be particularly useful.

[26] Shun-fu Gao, L. S. Celenza, Wei-Dong Sun, and J. Szweda, Brooklyn College Report No. BCCNT 95/981/249 (1995).